Lawrence Berkeley National Laboratory
LBL Publications

Title

Biogenic manganese oxides as reservoirs of organic carbon and proteins in terrestrial and marine environments

Authors

Estes, ER
Andeer, PF
Nordlund, D
et al.

ORIGINAL ARTICLE

WILEY gebiology

Biogenic manganese oxides as reservoirs of organic carbon and proteins in terrestrial and marine environments

E. R. Estes[1,2] | P. F. Andeer[2,3] | D. Nordlund[4] | S. D. Wankel[2] | C. M. Hansel[2]

[1]Department of Marine Chemistry and Geochemistry, MIT-WHOI Joint Program in Oceanography/Applied Ocean Science and Engineering, Woods Hole Oceanographic Institution, Woods Hole, MA, USA

[2]Department of Marine Chemistry and Geochemistry, Woods Hole Oceanographic Institution, Woods Hole, MA, USA

[3]Life Sciences Division, Lawrence Berkeley National Laboratory, Berkeley, CA, USA

[4]Stanford Synchrotron Radiation Lightsource, Menlo Park, CA, USA

Correspondence
C. M. Hansel, Department of Marine Chemistry and Geochemistry, Woods Hole Oceanographic Institution, Woods Hole, MA, USA
Email: chansel@whoi.edu

Abstract

Manganese (Mn) oxides participate in a range of interactions with organic carbon (OC) that can lead to either carbon degradation or preservation. Here, we examine the abundance and composition of OC associated with biogenic and environmental Mn oxides to elucidate the role of Mn oxides as a reservoir for carbon and their potential for selective partitioning of particular carbon species. Mn oxides precipitated in natural brackish waters and by Mn(II)-oxidizing marine bacteria and terrestrial fungi harbor considerable levels of organic carbon (4.1–17.0 mol OC per kg mineral) compared to ferromanganese cave deposits which contain 1–2 orders of magnitude lower OC. Spectroscopic analyses indicate that the chemical composition of Mn oxide-associated OC from microbial cultures is homogeneous with bacterial Mn oxides hosting primarily proteinaceous carbon and fungal Mn oxides containing both protein- and lipopolysaccharide-like carbon. The bacterial Mn oxide-hosted proteins are involved in both Mn(II) oxidation and metal binding by these bacterial species and could be involved in the mineral nucleation process as well. By comparison, the composition of OC associated with Mn oxides formed in natural settings (brackish waters and particularly in cave ferromanganese rock coatings) is more spatially and chemically heterogeneous. Cave Mn oxide-associated organic material is enriched in aliphatic C, which together with the lower carbon concentrations, points to more extensive microbial or mineral processing of carbon in this system relative to the other systems examined in this study, and as would be expected in oligotrophic cave environments. This study highlights Mn oxides as a reservoir for carbon in varied environments. The presence and in some cases dominance of proteinaceous carbon within the biogenic and natural Mn oxides may contribute to preferential preservation of proteins in sediments and dominance of protein-dependent metabolisms in the subsurface biosphere.

1 | INTRODUCTION

The availability of organic carbon (OC) to microbes is controlled by the concentration and composition of carbon and the geochemical parameters that control its reactivity. In oxygenated environments, OC not immediately remineralized by microbes is typically described as 'recalcitrant', generally implying that its molecular structure makes it intrinsically resistant to degradation. Molecular characterization of organic matter supports the idea of a reservoir of complex material (Hertkorn et al., 2006; Lechtenfeld et al., 2014; for instance) generated by either microbial processing, polymerization, or partial degradation reactions (Jiao et al., 2010 and references therein; Flerus et al., 2012; Johnson et al., 2015). Preservation of organic carbon, however, may be nonselective, whereby the chemical composition remains constant despite near-complete remineralization (Brandes et al., 2004; Cowie, Hedges, Prahl, & de Lange, 1995; Hedges et al., 2001) Further, presumed 'stable' OC is not necessarily inherently resistant to degradation (Carlson et al., 2004; Keil, Montluçon, Prahl, & Hedges, 1994; Kleber et al.,

2011). In aggregate, these studies imply that the chemical composition of OC itself is not a primary control on OC preservation and that there must be other underpinning biogeochemical mechanisms at play.

Physical and/or chemical protection of OC by minerals within soils and sediments is one such mechanism of preservation. In particular, the concentration and availability of OC can be substantially impacted by the mineralogical composition of soils/sediments and abundance of reactive mineral phases (Doetterl et al., 2015; Dümig, Häusler, Steffens, & Kögel-Knabner, 2012; Heckman, Vazquez-Ortega, Gao, Chorover, & Rasmussen, 2011; Keiluweit et al., 2015; Lalonde, Mucci, Ouellet, & Gélinas, 2012; Ransom, Kim, Kastner, & Wainwright, 1998), yet the underlying mechanisms remain unclear. While clays have historically been viewed as the primary control on mineral-hosted carbon (Arnarson & Keil, 2001; Bock & Mayer, 2000; Dickens et al., 2006; Dümig et al., 2012; Ransom et al., 1998), iron (Fe) oxides have more recently been shown to serve as a substantial sink for carbon in a wide range of marine and terrestrial environments and even in systems where Fe oxides are not considered stable (Kaiser & Guggenberger, 2000; Lalonde et al., 2012; Picard, Kappler, Schmid, Quaroni, & Obst, 2015; Poulton & Raiswell, 2005; Roy et al., 2013). Specifically, Fe oxides in marine sediments host an average of 20% of total organic carbon, levels that are disproportionally higher than their abundance (Lalonde et al., 2012). In addition to Fe oxides, manganese (Mn) oxides have a propensity to be associated with organic carbon (Johnson et al., 2015; Roy et al., 2013; Stone & Morgan, 1984; Sunda & Kieber, 1994) but have been less extensively studied. Carbon molecules can adsorb to mineral surfaces, serve as templates for mineral nucleation, and/ or coprecipitate with minerals during mineral growth and aggregation (Kleber et al., 2015; Mann et al., 1993; Moreau et al., 2007 and references therein). In fact, Fe(II)- and Mn(II)-oxidizing organisms utilize secreted organic molecules as templates for mineral growth (Chan, Fakra, Emerson, Fleming, & Edwards, 2011; Emerson, Garen, & Ghiorse, 1989) such that the association of certain biomolecule classes with oxide minerals may serve as a signature for biomineralization.

Conversely, metal oxides can serve as strong oxidants of organic matter (Stone & Morgan, 1984; Sunda & Kieber, 1994). In coastal sediments, comparison of carbon turnover rates with the residence times of Fe and Mn suggests that each metal atom experiences 100–300 redox cycles, often coupled to OC oxidation (Canfield, Thamdrup, & Hansen, 1993). Oxidized Mn species also drive microbially mediated litter decomposition in terrestrial systems (Berg et al., 2010; Keiluweit et al., 2015). In fact, both preservation and alteration of oxide-hosted carbon may take place, perhaps simultaneously, within a given deposit. Mn oxide deposits formed in a wastewater treatment facility contained alternating layers of Mn oxides and physically and chemically protected organic carbon; yet, evidence for OC degradation in that system pointed to simultaneous Mn oxide-induced carbon oxidation to low molecular weight OC (Johnson et al., 2015). Thus, these metal oxides appear to play an outsized role both in the preservation and in transformation of OC. Despite this, there remains a paucity of information on the abundance and composition of carbon associated with Mn oxides within biogenic precipitates and environmental systems, limiting our understanding of the underlying mechanisms and the potential role of such minerals as archives of organic molecules.

Accordingly, we investigated the concentration, distribution, and composition of organic carbon associated with environmental and biogenic Mn oxides. Mn(II)-oxidizing bacteria and fungi are considered primary organisms responsible for the formation of Mn oxides within marine waters and terrestrial sediments/rock coatings (Tebo et al., 2004). To explore potential differences in the concentration and chemical composition of organic carbon associated with Mn oxides in these environments, we characterized and compared OC-Mn oxide relationships within natural Mn oxides formed in brackish marine waters and a terrestrial cave system, as well as axenic cultures of representative Mn(II)-oxidizing organisms from each environment: two coastal marine bacteria (*Roseobacter* sp. AzwK-3b and *Erythrobacter* sp. SD-21) and two terrestrial fungi (*Pyrenochaeta* sp. DS3sAY3a and *Stagonospora* sp. SRC1IsM3a). This comparison provided insight into the range of OC-Mn oxide interactions that occur throughout mineral precipitation and preservation.

2 | MATERIALS AND METHODS

2.1 | Preparation of biological Mn oxide samples from Mn(II)-oxidizing cultures

Biogenic manganese oxides were precipitated by two alphaproteobacteria (*Roseobacter* sp. AzwK-3b and *Erythrobacter* sp. SD-21) and two ascomycete fungi (*Pyrenochaeta* sp. DS3sAY3a and *Stagnospora* sp. SRC1IsM3a). The two bacterial species are well-characterized Mn(II) oxidizers isolated from coastal surface sediments (*Erythrobacter*; Francis, Co, & Tebo, 2001) and a coastal estuary (*Roseobacter*; Hansel & Francis, 2006). The two fungi are cosmopolitan species found in a wide variety of terrestrial habitats that were isolated from Mn-rich wetlands treating coal mine drainage (Santelli et al., 2010).

Roseobacter sp. AzwK-3b was grown on J+acetate media consisting of 10 mM sodium acetate, 10 ml L^{-1} vitamin mix (in mg L^{-1}: biotin, 320; niacin, 32; thiamin, 16; 4-aminobenzoic acid, 32; calcium pantothenic acid, 16; pyridoxine, 160; vitamin B12, 16; riboflavin, 32; folic acid, 32), 1 ml L^{-1} 8% NH_4Cl, 2 mM $KHCO_3$, 0.2 ml L^{-1} 10% KH_2PO_4, and 3.6 μM iron (as $FeSO_4 \cdot 7H_2O$) complexed to 78 μM nitrilotriacetic acid, buffered to pH 7.6 with 20 mM HEPES, and prepared as 50% (volume) artificial seawater. *Erythrobacter* sp. SD-21 was grown in K-media (2 g L^{-1} peptone, 0.5 g L^{-1} yeast extract, buffered to pH 7.6 with 20 mM HEPES in 100% artificial seawater). Artificial seawater (Van Waasbergen, Hoch, & Tebo, 1993) contains 0.3 M NaCl, 0.05 M $MgSO_4 \cdot 7H_2O$, 0.01 M $CaCl_2 \cdot 2H_2O$, and 0.01 M KCl. Fungi were grown in AY media consisting of 0.25 g L^{-1} sodium acetate, 0.15 g L^{-1} yeast extract, 1 ml L^{-1} trace elements stock (in mg L^{-1}: $CuSO_4 \cdot 5H_2O$, 10; $ZnSO_4 \cdot 7H_2O$, 44; $CoCl_2 \cdot 6H_2O$, 20; $Na_2MoO_4 \cdot 2H_2O$; 13), and 20 mM HEPES buffer. All cultures were grown at room temperature under ambient light. The bacterial cultures were shaken (150 rpm), while fungi were grown under static conditions with occasional manual stirring.

Minerals were precipitated in cell-free filtrate following the procedure outlined in Learman et al. (2011). The bacterial cultures were grown to mid-log phase (as determined by absorption at 600 nm). Fungi were grown for either 8–10 days (*Stagonospora*) or 14 days (*Pyrenochaeta*), consistent with optimum Mn(II) oxidation capacity of their secretomes (Zeiner, 2015). Cultures were centrifuged at 4,000 *g* for 15 min and then filtered through a 0.2-μm PVDF membrane to produce cell-free filtrates. The cell-free filtrates were amended with 100 μM Mn(II) (from a stock solution of $MnCl_2 \cdot 4H_2O$) and shaken at 150 rpm at room temperature in the light for 6–96 hr, following the procedure optimized in Learman et al. (2011). Learman et al. (2011) demonstrated that 96 hr is sufficient for near-complete oxidation and for approximately 50% of the initial hexagonal birnessite phase to ripen into triclinic birnessite. For spectroscopic work, 200 μM Mn(II) was added to fungal filtrates. Previous characterization of the Mn oxides formed by fungi grown in liquid under these conditions produce solely hexagonal birnessite over the course of 96 hr (Santelli, Webb, Dohnalkova, & Hansel, 2011), but no time series were conducted for these species. In all experiments, reaction progress was tracked using the colorimetric reagent leucoberbelin blue (method described below).

At the end of the reaction period, precipitated minerals were collected by centrifugation (12,500 *g*) and then decanting the supernatant. Minerals were resuspended in a smaller volume of sterile DI water and transferred to 50-ml centrifuge tubes, pelleted a second time, resuspended in 2 ml sterile DI water, and transferred to microcentrifuge tubes. After a final centrifugation and decanting of supernatant, samples consisted of a mineral pellet in approximately 0.2 ml sterile DI. Previous experiments (data not shown) demonstrated that rinsing with DI is preferable to rinsing with natural water or media as the former does not affect the concentration or composition of mineral-associated OC as determined by element analyzer (EA, see below).

2.2 | Incubation experiments

2.2.1 | Biomineralization of Mn oxides in natural waters

Five to 10 L brackish water from Oyster Pond (Falmouth, MA) was collected from a depth of 1 meter twice in late May/early June 2014. A YSI 556MPS handheld multiparameter system was used to measure pH, conductivity, salinity, temperature, and dissolved oxygen in situ. Duplicate 40 ml subsamples for time zero (*t*0) measurements of dissolved organic carbon (DOC) were collected, filtered immediately through a 0.2-μm membrane, and acidified with 40 μl concentrated hydrochloric acid (HCl). In the laboratory, 500 ml aliquots of the unfiltered water were dispensed into sterile glass bottles and 100 μM Mn(II) (from a stock solution of $MnCl_2 \cdot 4H_2O$) added to each. Duplicate bottles were left at 25°C, still, and in the dark, to prevent photo-oxidation, for either 4 or 8 weeks.

At the end of the incubation period, Mn(II)-amended treatments had produced a large quantity of Mn oxide particles. Quantification was not possible as a portion of particles adhered to the sides of the bottles. Mineral samples were collected by filtering water through a

0.2-μm membrane, rinsing the membrane with sterile DI twice, and rinsing the particulate mineral and associated OC off the membrane into a microcentrifuge tube. As with the culture experiments, the final product consisted of a mineral pellet in approximately 0.2 ml sterile DI. Samples for DOC were taken from the filtrate and preserved as above.

2.2.2 | Adsorption of natural organic matter to synthetic Mn oxides

δ-MnO$_2$ was synthesized following the method described in Villalobos, Toner, Bargar, and Sposito (2003). Brackish water was collected from Oyster Pond in early September 2014 and analyzed at *t*0 for geochemical parameters as described above. Half the collected water was filtered through a 0.2-μm membrane ('0.2 μm filtered'), while the other half was left whole. 500 ml aliquots of the filtered and unfiltered water were amended with 100 μM synthetic δ-MnO$_2$ and incubated in the dark at 25°C for either 6 or 96 hr. At the end of the experiment, DOC and mineral samples were collected as in the biomineralization incubation experiments above.

2.3 | Cave site description and sample collection

Ferromanganese precipitates from Daniel Boone Caverns, a relatively pristine epigene karst cave in the Tennessee River Basin (Carmichael, Carmichael, Santelli, Strom, & Bräuer, 2013; Carmichael, Carmichael, Storm, et al., 2013), were collected in June 2014. Mn oxides form within biofilms, as coatings on rocks in pools or under seeps, as crusts along cave walls and speleothems, and as particles within mud formed by mineral weathering processes. Mn oxide-coated rock samples were taken at two sites where coatings were actively forming under pooled water. Samples were placed in sterile centrifuge tubes or sample bags; coatings utilized in analyses were removed from the rock surface in laboratory using a sterile razor blade after mud was removed using sterile ultrapure water.

2.4 | Quantification of Mn(III/IV) oxides

Mn(III/IV) oxide concentrations were quantified at 620 nm (Cary 60 UV–Vis spectrophotometer, Varian) using the colorimetric reagent leucoberbelin blue (LBB, Sigma; Krumbein & Altmann, 1973) which reacts with both Mn(III) and Mn(IV). Concentrations were calibrated using a permanganate standard (KMnO$_4$, EDM). A conversion factor of 2.5 was used, as 1 M KMnO$_4$ can oxidize 5 M LBB relative to the 2 M LBB oxidized by a Mn(IV) oxide. This calculation assumes that the Mn oxide is 100% Mn(IV), which is largely consistent with the Mn(IV)-dominated δ-MnO$_2$ phases observed for the cultures (as indicated above and in Learman et al. (2011) and Santelli et al. (2011)) and the Oyster Pond incubations and cave deposits (see Results below). However, for samples containing triclinic birnessite, the Mn(III) content can be higher. Thus, this LBB conversion factor would result in an underestimation of Mn oxide concentrations for samples containing triclinic birnessite. To quantify Mn

oxides in cave samples, 3–10 mg of dried and ground ferromanganese deposit from each sample was weighed in duplicate and reacted with 2 ml LBB reagent for 15 min with periodic shaking. The reacted solution was then filtered through a 0.2-μm membrane and analyzed.

2.5 | Spectroscopic analysis of Mn oxides

Extended X-ray absorption fine structure (EXAFS) spectroscopy was conducted on beamline 4-3 at the Stanford Synchrotron Radiation Lightsource (SSRL) to determine the structure of the natural Mn oxides. Measurements were made using a Si(111) monochromator ($\Phi = 90°$) and calibrated with a $KMnO_4$ standard (6543.34 eV). Fluorescence data were collected with a Vortex silicon drift detector, with 3–4 scans per sample taken at room temperature from about −200 to +1000 around the Mn K-edge (6539 eV). Data processing was conducted using the SIX-PACK software program (Webb, 2005a, 2005b). XAS scans were averaged, background-subtracted, normalized, and converted to $\chi(k)$ spectra. Spectra were k^3-weighted and fit using a k range of 3–12 $Å^{-1}$, as a substantial Fe K-edge was observed in the natural samples. Linear combination fitting was performed as described in detail in Learman et al., 2011 and Bargar et al., 2005; using δ-MnO_2, Na–birnessite, acid birnessite, groutite (α-MnOOH), feitknechtite (β-MnOOH), hausmannite (Mn_3O_4), Na–buserite, synthetic todorokite ((Na, Ca, K)(Mg, Mn)Mn_6O_{14}•$5H_2O$), pyrolusite (β-MnO_2), manganese iron oxide ($MnFe_2O_4$), groutite (Mn(III)OOH), 10-Å manganate, rhodochrosite ($MnCO_3$), and aqueous $MnSO_4$ as model compounds.

2.6 | Carbon spectroscopic analyses

Scanning transmission X-ray microscopy (STXM) coupled to NEXAFS spectroscopy was conducted on beamline 11.0.2 at the Advanced Light Source (ALS). The STXM end station uses Fresnel zone plates to focus the monochromatic X-ray beam and plane grating monochromator to resolve the energy. Mineral samples (1–10 μl) were pipetted onto silicon nitride membranes (Si_3N_4, Silson, Ltd., Northampton, England) and air-dried. For each sample, 200 × 200 μm transmission images were used to find a region that was not too optically dense. Then, optical density (OD) maps ranging between 50 × 50 and 15 × 15 μm in size were taken over the C, N, Al, and Si K-edge and the Mn and Fe L_3 edge, with OD = ln (I_0/I), and maps achieved by subtracting a pre-edge transmission image from a post-edge image. Finally, a C K-edge stack was collected from 279 to 320 eV at step sizes as small as 0.1 eV, a dwell time of 1 ms, and a spatial resolution of 75–100 nm. Image processing, alignment, and i0 normalization was conducted using the IDL package aXis2000. Regions of interest were selected based on sample morphology and element distributions as observed in element OD maps and C NEXAFS spectra extracted. Between 4 and 12, spectral regions were extracted per sample; representative regions were selected for analysis in this work. Spectra were imported into Igor Pro and intensity normalized.

2.7 | NEXAFS peak deconvolution

Gaussian deconvolution of spectra from both bulk NEXAFS and STXM-NEXAFS was conducted using PeakFit software (SeaSolve Software Inc., San Jose, CA, USA) and following the peak assignments and parameters described in Keiluweit et al. (2012) and references therein. In brief, spectra were fit using six Gaussian peaks corresponding to approximate positions of major functional group resonances, according to the convention followed in the literature (Keiluweit et al., 2012; Kleber et al., 2011; Schumacher, Christl, Scheinost, Jacobsen, & Kretzschmar, 2005; Solomon, Lehmann, Kinyangi, Liang, & Schafer, 2005). Peak magnitude and energy were allowed to vary freely and always constrained themselves to the energy ranges expected for each functionality. As in previous works (Keiluweit et al., 2012; Kleber et al., 2011), the ionization threshold was fit using a 'transition' function in PeakFit set at 290 eV that approximates the arctangent function used by other researchers (Solomon et al., 2005), while σ^* transitions were fit with two additional Gaussians. Fit results were expressed as 'percent of the fit area', excluding the transition function and σ^* Gaussians as they were above the energy range of interest and did not affect peak areas.

2.8 | Quantification of organic carbon

Mineral-associated OC was quantified via elemental analyzer (elementar vario PYRO cube, Hanau, Germany). Freeze-dried, weighed samples were analyzed in triplicate as sample material allowed. Concentration calibrations were made using NIST-certified standard USGS40 L-glutamic acid as well as Na–EDTA diluted tenfold in silicon dioxide (Unimin, Spruce Pine, NC) and homogenized. A set of four standards were run every 10–12 samples to correct for size and drift. Cave samples were analyzed in quadruplicate. These samples were weighed into silver boats, wet with 20 μl ultrapure water, and acid fumed in a desiccator with a beaker containing 50 ml concentrated hydrochloric acid for 24 hr to remove inorganic carbon. Following this procedure, samples were dried at 60°C for 12 hr and folded into a second silver boat.

Protein associated with Mn oxides was quantified using Qubit fluorescent reagent (Life Technologies) and calibrated using BSA standards (Bio-Rad). Proteins were removed from mineral surfaces by suspending the sample in 1.5 ml ultrapure water and sonicating three times at 40% duty cycle, keeping the samples on ice between sonication cycles. 300 μl of 6N hydrochloric was then added to the solution and incubated at 37°C for 30 min. Then, 75 μl 10 M trichloroacetic acid was added, and the mixture incubated on ice for 30 min. Finally, samples were spun down, the supernatant transferred, and an additional 500 μl of 0.1 N NaOH was added. Samples were boiled for 5 min and cooled to room temperature prior to analysis. (Protocol modified from Ehrenreich and Widdel (1994)).

2.9 | Protein extraction and identification

Protein extractions were performed on rinsed, concentrated Mn oxide minerals collected from cell-free filtrate of both *R.* AzwK-3b and *E.* SD-21 cultures embedded in polyacrylamide gel. Protein digestions followed a protocol adapted from Lu and Zhu (2005). Because metals interfere with acrylamide polymerization, the Mn oxide slurry (87 μl) was not mixed with the acrylamide solution (103 μl of 30% acrylamide diluted in 1 M Tris) until ~30 s after the addition of TEMED (3 μl), ammonium persulfate (7 μl of 1% solution), and LCMS grade water (37 μl). The DTT (10 mM) incubation and washing steps in the protocol were sufficient to remove the Mn oxides prior to digestion with trypsin (20 μg ml^{-1}, Promega). Following digestion, extracted proteins were purified and concentrated by binding to a C$_8$ frit (Michrom) and eluted with acetonitrile (Sigma Aldrich). Due to concerns about low protein concentrations, samples were not controlled for mass and therefore peptide abundances are not comparable between samples. Purified samples were analyzed using an LTQ XL linear ion trap mass spectrometer in the Woods Hole Oceanographic Institution Mass Spectrometer Facility as described previously (Andeer, Learman, McIlvin, Dunn, & Hansel, 2015). Peptides were then compared to sequences for *Roseobacter* AzwK-3b or *Erythrobacter* SD-21, respectively, using Bioworks v3.3.1 SP1 (Thermo Scientific) and further analyzed using Scaffold v4 (PROTEOME Software). A blank containing the sterile ultrapure water used in the mineral rinsing procedure was also analyzed.

3 | RESULTS

3.1 | Mn oxide characterization

Mn oxides formed by the Mn(II)-oxidizing bacteria and fungi explored here and grown under similar conditions were identified as a nanocrystalline hexagonal birnessite phase similar to δ-MnO$_2$ in previous investigations (Learman et al., 2011; Santelli et al., 2011). For *Roseobacter* AzwK-3b, however, the initial hexagonal birnessite phase is colloidal and ripens to a larger particulate triclinic birnessite phase over 96 hr (Learman et al., 2011).

Incubation of Oyster Pond water with aqueous Mn(II) led to visible Mn oxide particles starting after approximately 4 weeks. Linear combination fitting of the Mn EXAFS spectra revealed that the Mn oxides precipitated after 4 weeks consisted of hexagonal birnessite similar to δ-MnO$_2$ with a small contribution from either adsorbed or structurally bound Mn(II) (8%; Fig. S1 and Table S1). After 8 weeks, the Mn oxides remain as primarily hexagonal birnessite, but contain more Mn(II) (12%) and a substantial amount of triclinic Na-birnessite (38%) (Fig. S1 and Table S1).

The cave ferromanganese deposits, unlike the axenic cultures and brackish water incubations, contained a mixture of oxide and non-oxide mineral phases (carbonates, clays). Concentrations of Mn(III/IV) in ferromanganese rock coatings forming in two different pools within Daniel Boone Caverns, Cliff Ledge and Bacon Cove, were therefore determined to be 12.8 and 31.4 mmol Mn oxide per kg solid, respectively. Linear combination fitting of Mn EXAFS spectra collected of the ferromanganese coating samples indicated that the solid-phase Mn is dominated by δ-MnO$_2$ (92%–93%) with the remaining either adsorbed or structurally incorporated Mn(II) (Fig. S1 and Table S1).

3.2 | Carbon quantification

Manganese oxides formed in the cell-free filtrate of *Roseobacter* AzwK-3b and *Erythrobacter* SD-21 harbored a substantial amount of organic carbon (Fig. 1). After 96 hr, the OC concentration associated with the *Roseobacter* Mn oxides was 8.50 ± 0.84 mol OC per kg mineral. In comparison, Mn oxides formed in the *Erythrobacter* filtrate contained significantly more OC (17.00 ± 0.43 mol OC per kg mineral) than that accumulated by *Roseobacter* Mn oxides over the same time frame ($p < .001$, two-tailed t test).

Mn oxides formed with cell-free filtrate from the fungi *Pyrenochaeta* sp. DS3sAY3a and *Stagonospora* sp. SRC1lsM3a also harbored organic carbon (Fig. 1). The concentration of carbon associated with Mn oxides precipitated by *Stagonospora* sp. and *Pyrenochaeta* sp. was 5.34 ± 0.45 and 4.15 ± 0.44 mol OC per kg mineral, respectively, levels that are significantly lower than those observed for the bacterial Mn oxides ($p < .001$, one-way ANOVA; Fig. 1).

Mn oxide precipitates formed via Mn(II) oxidation within Oyster Pond water incubated for 4 and 8 weeks contained 11.4 ± 0.3 and 6.2 ± 2.0 mol OC per kg mineral, respectively—levels that are similar to those measured for the fungal and bacterial cultures (Figs 1 and S2). The amount of OC associated with synthetic Mn oxides added to the Oyster Pond water was 3.4 ± 0.1 and 5.0 ± 0.1 mol OC per kg mineral after 96 hr and 4 weeks, respectively (Fig. 2). The DOC associated with
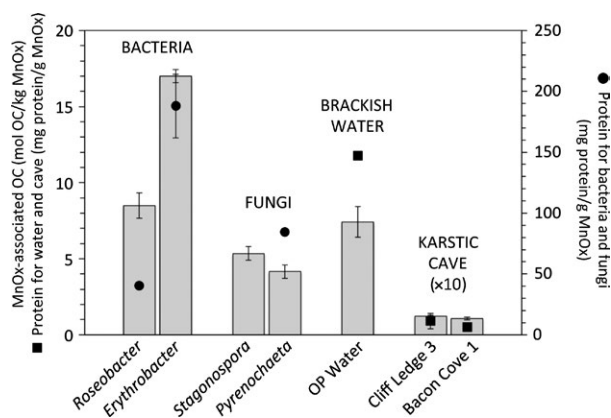
FIGURE 1 Organic carbon and protein concentrations associated with Mn oxides formed in the cell-free filtrate of bacterial and fungal cultures. Bacterial and fungal samples came from 96-hr incubations, while the brackish Oyster Pond water sample was incubated for 8 weeks. The *Stagonospora* sample did not contain enough volume to allow measurement of proteins. TOC and protein concentrations for cave samples are multiplied 10× such that they are visible on the graph

the synthetic Mn oxides added to filtered (0.2 μm) water after 96 hr of incubation was 1.8 ± 0.1 mol OC per kg mineral. The initial DOC concentration within the Oyster Pond water was 0.74 ± 0.02 mmol DOC L^{-1}.

Ferromanganese rock coatings from the karstic cave system contain 1–2 orders of magnitude less OC than the Mn oxides formed by axenic cultures or Oyster Pond water incubations (Fig. 1). Concentrations of total organic carbon associated with the rock coatings
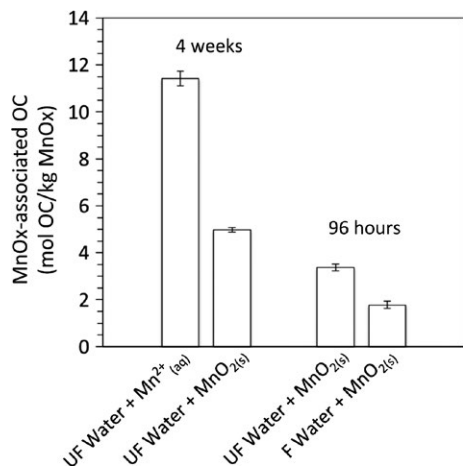
FIGURE 2 Organic carbon concentrations associated with Mn oxides following different incubation treatments in brackish Oyster Pond water: Mn oxides formed from Mn(II) over the course of 4 weeks (UF Water + Mn^{2+}$_{(aq)}$), synthetic Mn oxides incubated for 4 weeks (UF Water + MnO$_2$), synthetic Mn oxides incubated for 96 hr (UF Water + MnO$_2$), and synthetic Mn oxides incubated in 0.2 μm filtered water for 96 hr (F Water + MnO$_2$)

(although not explicitly mineral associated) ranged from 0.107 ± 0.009 to 0.123 ± 0.007 mol OC per kg solid.

3.3 | Mn oxide–organic carbon associations and carbon composition

A clear association between bacteriogenic and mycogenic Mn oxide particles and organic carbon was visually observed via STXM (Fig. 3). STXM C and Mn optical density (OD) maps demonstrated close spatial correlation between carbon and Mn oxide minerals formed in *Roseobacter* and *Erythrobacter* cell-free filtrate (Fig. 3, left panel). The chemical composition of the organic carbon associated with the biogenic Mn oxides produced in both the *Roseobacter* and *Erythrobacter* axenic cultures was spatially homogeneous. C NEXAFS spectra extracted from four different regions of the STXM-NEXAFS stacks for each organism, as denoted on the Mn and C OD maps, appeared nearly identical despite variations in sample morphology and relative Mn and C density (Fig. 3, top right panel). The C NEXAFS spectrum from region 2a of the *Erythrobacter* Mn oxides was particularly enriched in amide/carboxylic C (~288.3 eV), but otherwise appeared similar to regions 2b–d. For the primary functional groups (aromatic, aliphatic, amide/carboxylic, and O-alkyl-carbon), average relative standard deviation between regions within a sample was ~10%, demonstrating homogeneity and reproducibility. Overall, *Erythrobacter* Mn oxides contained about half as much aromatic C as *Roseobacter* Mn oxides, comparable contributions from aliphatic and amide/carboxylic C, and slightly more O-alkyl-C than *Roseobacter* Mn oxides (Table S2).

As chemical composition appeared spatially homogeneous, a spectrum was extracted from the entire particle. This 'total' C spectral

FIGURE 3 Mn and C STXM OD maps of Mn oxides formed in cell-free filtrate of bacterial and fungal cultures (left) generated by subtracting a pre-edge transmission image from a post-edge image (see Methods). C 1s NEXAFS spectra (right) extracted from regions denoted on the STXM maps. Lower right panel expands spectra taken from *Stagonospora* Mn oxides. Guide lines are at 285.3, 287.4, 288.3, and 289.45 eV
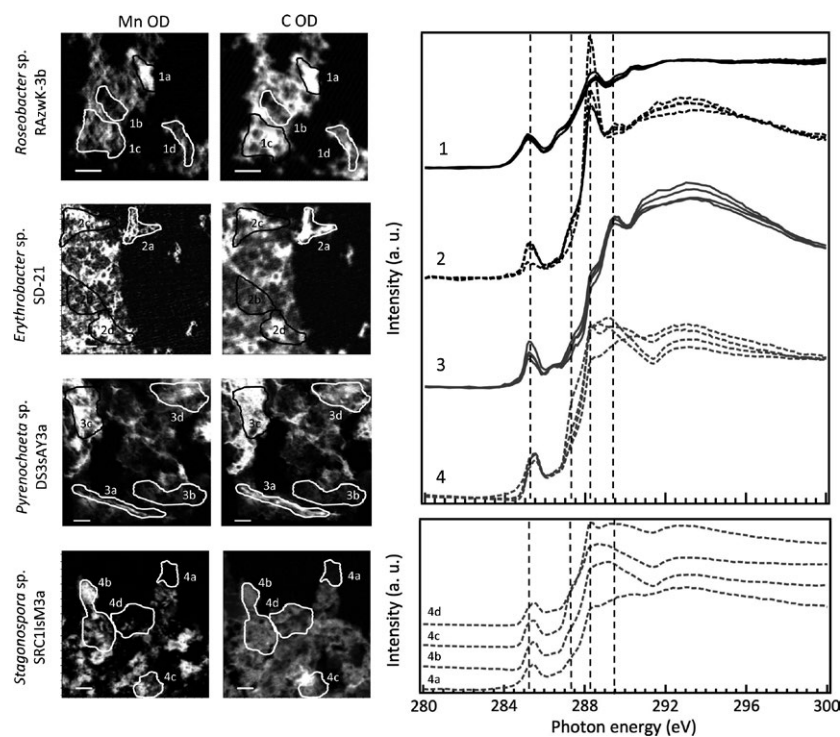
signature for Mn oxides produced both in the *Roseobacter* and in *Erythrobacter* filtrate was most similar to a protein standard, containing peaks corresponding to aromatic, aliphatic, and amide/carboxylic C (Fig. 4) and with an average amide/carboxylic C contribution of 44% ± 2% (Fig. 5; Table S2). Bulk carbon 1s NEXAFS spectra for *Roseobacter* Mn oxides (Fig. S3) as well as *Erythrobacter* Mn oxides (not shown) were consistent with the STXM spectra (Fig. 4). Nitrogen 1s NEXAFS (Fig. S3, right panel) confirmed the identification of OC associated with Mn oxides precipitated by *Roseobacter* as a protein,
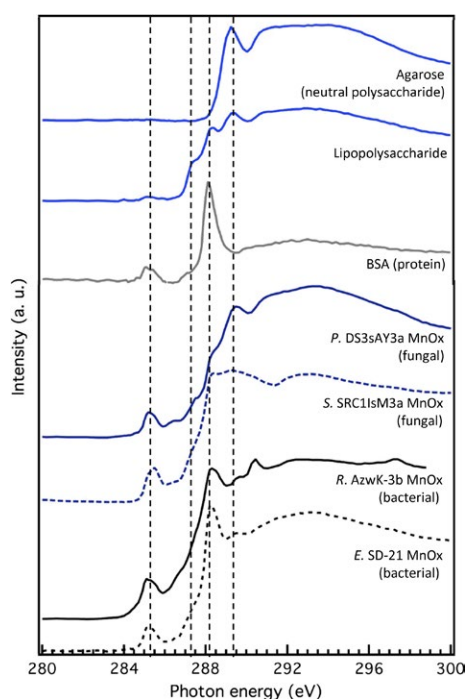
with the primary N-NEXAFS peak at 401.4 eV corresponding to amide N (Fig. S3). The C NEXAFS spectra of Mn oxides from *Roseobacter* and particularly *Erythrobacter* contained an additional contribution from O-alkyl-C groups at ~289.4 eV, which is not found in the protein standard.

NEXAFS spectra extracted from four different regions of the STXM-NEXAFS stacks appeared nearly identical for *Pyrenochaeta* sp. (Fig. 3, top right panel). However, spectra extracted from morphologically distinct regions of the *Stagonospora* sp. Mn oxides differed slightly, as shown in the bottom right panel of Fig. 3. These differences derive from peak intensities rather than peak positions or the presence/absence of certain peaks. Region 4a is relatively Mn and C poor and contained less aliphatic and O-alkyl-C groups and more amide/carboxylic C than the other regions, based on peak fitting results, although these differences were not substantial (Table S2). Regions 4b and 4c were both Mn and C rich and have more distinct shoulders at ~287.3 eV, corresponding to aliphatic C. Peak fitting results nonetheless demonstrated that *Pyrenochaeta* sp. and *Stagonospora* sp. Mn oxides were similar to each other in overall composition, only differing significantly in their O-alkyl-C content (~289.3 eV, *p* = .038, one-way ANOVA; Table S2). In fact, for the most prominent functional groups (aromatic, aliphatic, amide/carboxylic, and O-alkyl-C), the average relative standard deviation was 11.8% across all regions of both fungal samples.

Carbon associated with the two mycogenic Mn oxide precipitates had a distinctly different C NEXAFS signature from the bacterial oxides and was specifically more similar to the lipopolysaccharide and neutral polysaccharide standards (Fig. 4). The sample spectra were defined by shoulders for aliphatic C (~287.3 eV, average 7.2% ± 0.6% of total area) and amide or carboxyl C (~288.3 eV, average 25.6% ± 3.0%), rising to a primary peak corresponding to O-alkyl-C at ~289.3–289.5 eV (average 42.9% ± 2.5%). Both mycogenic Mn oxide samples harbored carbon with a greater contribution from aromatic groups (~285.4 eV, average 7.7% ± 0.4%) and lower aliphatic C than pure lipopolysaccharides, but the match was otherwise strong in overall spectral shape and contribution of functional groups (LPS contains: aromatic C, 0.8%;

FIGURE 4 Representative C 1s NEXAFS spectra of carbon associated with Mn oxides precipitated in the cell-free filtrate of fungal (blue) and bacterial cultures (black) generated by extracting the entirety of the STXM image for each species, shown with matching standards. Guidelines are at 285.3, 287.4, 288.3, and 289.45 eV
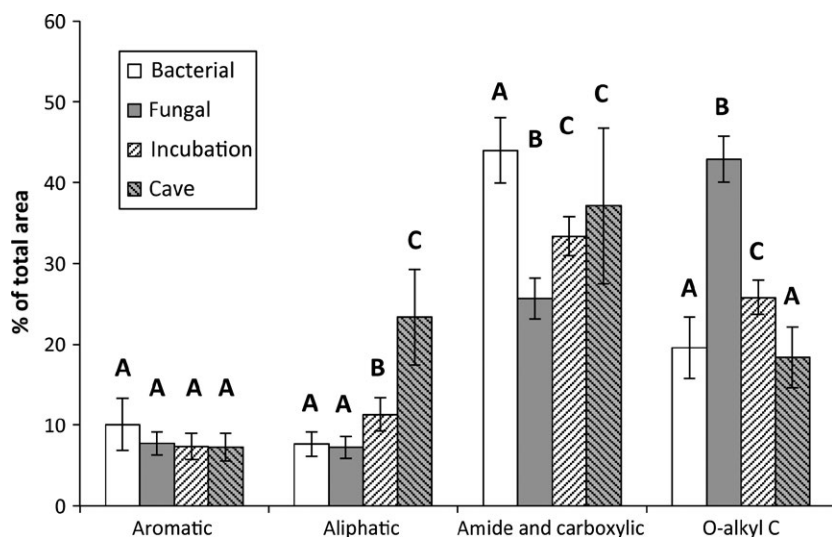
FIGURE 5 Average percent contribution of primary functional groups to total spectral area. Statistical differences determined by one-way ANOVAs. Letters designate significant differences between sample types (*p* < .05, see text)
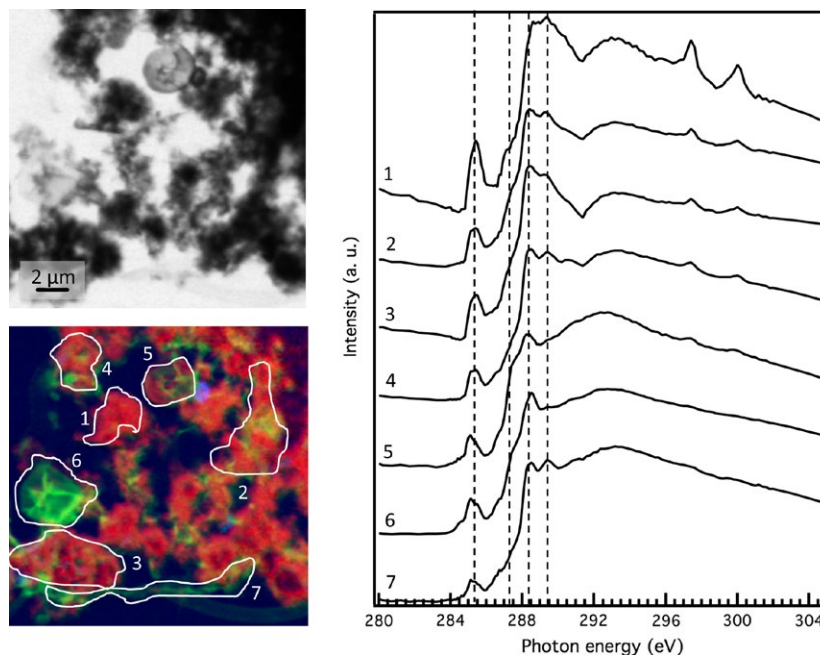
FIGURE 6 Transmission image (top left) and C (green), Mn (red), and Fe (blue) overlaid STXM OD maps of Mn oxides formed in Oyster Pond brackish water after 8 weeks (bottom left) and corresponding C 1s NEXAFS spectra (right). Guide lines are at 285.4, 287.2, 288.4, and 289.45 eV

aliphatic C, 25.9%; amide/carboxylic C, 42.3%; O-alkyl-C 13.8%). The greater contribution from O-alkyl-C and the more minor contribution from amide and carboxylic C in the fungal samples compared to the lipopolysaccharide standard likely reflected a component of neutral polysaccharides, as fitting revealed that the agarose standard is comprised of 75.2% O-alkyl-C and no amide/carboxylic C (Fig. 4; Table S2). In contrast to the average OC composition of bacterial Mn oxides, then, mycogenic Mn oxides contained significantly less phenolic/ketonic C ($p = .04$, one-way ANOVA), less amide/carboxylic C ($p < .001$, one-way ANOVA), and more O-alkyl-C ($p < .001$, one-way ANOVA; Fig. 5, Table S2).

Similar to Mn oxides formed by axenic bacteria and fungi (Fig. 3), both synthetic and actively biomineralized Mn oxides formed within the coastal water incubations had a close association with carbon (Figs 6 and S4). Overlaid Mn, C, and Fe OD maps (red, green, and blue, respectively) of Mn oxides formed in the unfiltered Oyster Pond water incubated for 8 weeks revealed some particulate organic C not associated with Mn oxides (regions 6 and 7, green only) as well as some accumulated Fe (blue), but an overall spatial correlation in the distribution of Mn and C.

In contrast to the biogenic Mn oxides formed in the axenic cultures, Mn oxides formed within the Oyster Pond water incubations contained carbon with a more spatially heterogeneous chemical composition (Fig. 6). C NEXAFS spectra extracted from distinct regions showed a diversity of spectral signatures that could not be matched with individual standard compounds. Instead, the spectra contained a variety of spectral features indicative of a more complex carbon composition. Regions where carbon was associated with Mn oxides had similar spectral signatures (8-week incubation, excluding C-only regions 6 and 7). C NEXAFS spectra from these regions showed the presence of aromatic, aliphatic, amide/carboxylic, and O-alkyl-C carbon (285.4, shoulder at ~287.3, ~288.4, and ~289.4 eV, comprising

7.3% ± 1.6%, 11.3% ± 2.1%, 33.3% ± 2.4%, and 25.7% ± 2.1% of the total fit area, respectively), with the peak corresponding to amide/carboxylic C making the greatest contribution to fit area (Fig. 5, Table S2). Two regions (6 and 7) were composed of particulate carbon not associated with Mn (Fig. 6). Like the Mn-bearing regions in this sample, the peak corresponding to amide/carboxylic C still made the largest contribution to overall fit area, at 36.0%± 4.2% (Table S2). These two regions differed from each other as much as from the Mn-bearing regions; region 6 had the highest aliphatic content of all analyzed regions (14.5%) and region 7 the lowest (5.9%), while the relative contribution to fit area of the other functional groups fell within the same range as the Mn-bearing regions.

Scanning transmission X-ray microscopy elemental mapping of two cave samples showed distinct regions for each element with a lesser degree of C-Mn coupling (Fig. 7, left panel) than observed in the culture and water incubation samples (Figs 3 and 6). In sample 'Bacon Cove 1', Mn-rich regions also contained C, which in some instances was observed as what appears to be a coating around a particle (see bottom middle particle in map, Fig. 7). Particulate carbon was also observed that was not associated with Mn. Iron regions are closely aligned with Mn, and thus, this particulate carbon was either not mineral associated or the minerals did not contain Fe or Mn. Si maps also did not overlap with this particulate carbon (not shown). Unlike Bacon Cove, Mn, and Fe were distributed as discrete particles in sample 'Cliff Ledge 3', with both Mn-rich and Fe-rich particles bearing associated carbon, including coatings along the mineral grains. The samples also contained a substantial amount of C, both organic and inorganic, that was not associated with Mn- and Fe-rich regions. Some of the visible C associated with Si-bearing phases, but these were often too optically dense to extract spectra from.

C NEXAFS spectra extracted from various regions of the cave samples had similar spectral features to the biogenic Mn oxides
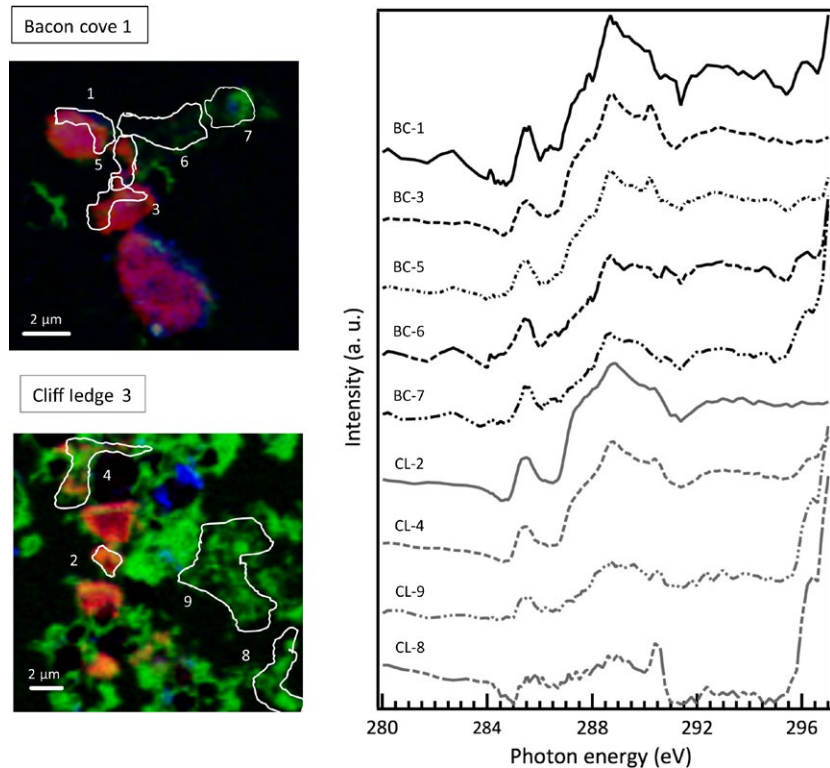
FIGURE 7 C (green), Mn (red), and Fe (blue) overlaid STXM OD maps of cave ferromanganese rock coatings (left) and corresponding C 1s NEXAFS spectra (right) for samples Bacon Cove 1 (top, black spectra) and Cliff Ledge 3 (bottom, gray spectra)

from the cultures and coastal water incubations, including a peak identified as aromatic C at ~285.5 eV, a shoulder corresponding to aliphatic C around 287.4 eV, a primary amide/carboxylic C peak at ~288.6 eV, and a minor feature at ~289.6 eV identified as O-alkyl-C functional groups (Fig. 7 right panel). Several of the regions contained inorganic carbon, identified by the sharp peak between 290.2 and 290.6 eV. Based on peak fitting results, however, inorganic C accounted for only 4%–18% of the total carbon in all regions (Table S2).

To look for differences in OC composition between spectra, regions were averaged either by site or by whether the region represented Mn oxide-associated OC or bulk OC. By site, Cliff Ledge had a higher content of amide/carboxylic C (~288.6 eV, $p = .031$, two-tailed t test, 41.5% ± 9.3% relative to 31.5% ± 1.0%) but lower aliphatic C (~287.5 eV, $p = .004$, two-tailed t test, 17.1% ± 1.6% compared to 25.1% ± 3.4% of total fit area; Table S2). When classified as Mn oxide–OC or bulk OC, the C-rich regions that did not contain Mn had higher aromatic and phenolic/ketonic C (~285.4 eV, $p = .010$, two-tailed t test, 11.3% ± 1.7% relative to 7.3% ± 1.7% and ~286.4 eV, $p = .012$, two-tailed t test, 3.2% ± 0.8% relative to 1.1% ± 1.0%; Table S2) but had no other significant differences.

Overall, the most striking difference between spectra extracted from the ferromanganese coating samples relative to bacterial/fungal and Oyster Pond Mn oxides was the contribution from aliphatic C groups (~287.3–287.5 eV). Averaging peak fitting results from all regions extracted from each sample type together showed that OC in cave samples contains 22% ± 5% aliphatic groups relative to 11% ± 3% and 7% ± 1% for the incubation and culture samples, respectively ($p < .001$, one-way ANOVA; Fig. 5, Table S2).

3.4 | Protein quantification

For some samples, enough material was obtained to specifically quantify the proteins associated with the Mn oxides (Fig. 1). Within the *Roseobacter* filtrate, the concentration of proteins associated with the Mn oxides was 40.24 ± 1.12 mg protein per g mineral after 96 hr of incubation. Similar to OC, Mn oxides formed within the *Erythrobacter* filtrate contained significantly more protein (187.96 ± 26.18 mg protein per g mineral) than the *Roseobacter* Mn oxides after 96 hr ($p < .001$, two-tailed t test).

Not enough biogenic Mn oxides were recovered to allow for quantification of the proteins associated with *Stagonospora* sp. Mn oxides, but *Pyrenochaeta* sp. Mn oxides contained 84.55 mg protein per g mineral (Fig. 1), proportionally more of the OC pool than that found associated with bacterial Mn oxides.

The concentration of OC associated with Mn oxides formed via Mn(II) oxidation within the Oyster Pond water after 8 weeks was 11.8 mg protein per g mineral (Fig. 1).

For the cave samples, protein concentrations are several orders of magnitude lower than that associated with Mn oxides formed in axenic cultures, ranging from 0.05 ± 0.01 (Bacon Cove) to 0.09 ± 0.05 (Cliff Ledge 3) mg protein per g mineral (Fig. 1).

3.5 | Protein identification

As proteins were the primary form of OC associated with bacterial Mn oxides based on C- and N-NEXAFS spectroscopy, we extracted and identified the Mn oxide-harbored proteins to gain insight into the types of proteins present in the minerals. The majority of

peptides identified in the *Roseobacter* sp. AzwK-3b Mn oxide minerals (>55%, Table S3) were associated with animal heme peroxidases (AHPs) encoded by its genome (Andeer et al., 2015). Several other proteins were identified in the *Roseobacter* extractions, but were detected at much lower relative abundances (as measured by relative spectrum counts). The Mn oxide minerals generated by *Erythrobacter* sp. SD-21 also contained a homolog to the AHPs found in *Roseobacter*, MopA (Dick et al., 2008). However, several other proteins were also identified in these Mn oxide minerals with similar spectral counts to MopA (ca. 7.9%).

In addition to these peroxidases, there were several other Mn oxide-associated proteins involved with ion binding or transport. One such protein in the *Roseobacter* Mn oxides was a putative metal permease belonging to a family associated with the cellular uptake of Mn^{2+} and Zn^{2+} (Claverys, 2001). Also identified were a pair of hemolysin proteins that belong to a family of proteins that are capable of binding Ca^{2+} and Zn^{2+} (Ostolaza, Soloaga, & Goni, 1995). Many TonB receptor family proteins, which are involved with the uptake of substrates such as iron complexes (Koebnik, Locher, & Van Gelder, 2000), along with a number of proteases and peptidases, including at least one putative metalloprotease, were identified in the *Erythrobacter* Mn oxides. While most metalloproteases are associated with Zn, examples of proteases with improved activity when bound to manganese (Graham, Bond, Freeman, & Guss, 2005) or in the presence of manganese (Kuddus & Ramteke, 2008) have been reported.

4 | DISCUSSION

Mn oxides formed within brackish water incubations and as cave ferromanganese rock coatings are composed of δ-MnO_2, a poorly ordered layered birnessite phase, similar to the Mn oxides formed by the bacterial and fungal cultures (see Learman et al., 2011; Santelli et al., 2011). δ-MnO2 is the primary type of Mn oxide formed by micro-organisms (Bargar et al., 2005; Santelli et al., 2011; Webb, 2005b) and within near-surface environments (review by Tebo et al., 2004 and references therein, Bargar et al., 2009). Similar to *Roseobacter* Mn oxides, the hexagonal birnessite phase formed in the brackish water incubations ripens to a more crystalline triclinic birnessite phase over several weeks (Fig. S1, Table S1).

These biogenic and natural Mn oxides harbor substantial concentrations of organic carbon, ranging from 4.2 to 17.0 mol OC per kg solid in bacterial and fungal cultures and brackish pond water incubations (Fig. 1). In contrast, cave ferromanganese deposits host far less OC (0.09–0.12 mol OC per kg solid; Fig. 1). By assigning an approximate formula of MnO_2 to culture- and brackish water-derived Mn oxides, an OC:Mn ratio (mol:mol) can be calculated and ranges from 0.36 to 1.47. For cave samples, we calculate an OC:Mn of 2.99–8.37, but these values are artificially high as they reflect TOC and not just Mn oxide-associated OC. Nonetheless, the magnitude and range of OC:Mn observed in this study are consistent with other carbon–metal deposits, including Mn oxide deposits in a wastewater treatment

facility (>0.22 OC:Mn; calculated from Johnson et al., 2015), estuarine and deltaic sediments (OC:Fe of 0.2–4.72, reported by Lalonde et al., 2012), hydrothermal plume particles (OC:Fe + Mn ~2.69–17.8 calculated from Toner et al., 2009), and DOM removal by Fe-based coagulants (OC:Fe 1.9–3.5, Henneberry, Kraus, Nico, & Horwath, 2012).

Within axenic microbial cultures, uniform and distinct carbon signatures are observed for marine bacteria versus terrestrial fungi (Figs 3 and 4). Specifically, OC associated with marine bacterial Mn oxides is primarily proteinaceous (Figs 4 and S3), while terrestrial mycogenic Mn oxides harbor both protein and (lipo)polysaccharide-like material (Fig. 4). These signatures could derive from amino sugars, which would produce spectra with strong peaks corresponding to both amine C and O-alkyl-C (Solomon et al., 2009). However, the spectra closely match protein and/or lipopolysaccharide standards (for bacterial and fungal Mn oxides, respectively) and the additional N-NEXAFS (Fig. S3), protein quantification (Fig. 1), and protein extraction and identification data (Table S3) for the bacterial samples affirm this interpretation. These and closely related organisms are known to have extensive secretomes (Christie-Oleza, Piña-Villalonga, Bosch, Nogales, & Armengaud, 2012; Johnson, Soule, & Kujawinski, 2016; Learman & Hansel, 2014; Zeiner, 2015); thus, while amino sugars could be present and associating with the mineral, it is not surprising to find that Mn-associated OC derives from extracellular proteins and lipopolysaccharides.

While the organic carbon composition of the initial growth media varied between the cultures, the fungal and *Erythrobacter* sp. media is quite similar and therefore cannot account for the differences observed between these organisms. Further, ascomycete fungi, including the two species explored here, have extensive exoproteomes (Zeiner, 2015 and references therein), and yet their Mn oxides are dominated by a (lipo)polysaccharide signature. As the type and structure of the Mn oxides formed by these bacteria and fungi are similar (Learman et al., 2011; Santelli et al., 2011), these findings could point to specific biomolecules involved in Mn biomineralization by bacteria versus fungi. However, a range of polysaccharides, proteins, and specific amino acids has been implicated in the nucleation, precipitation, and aggregation of a wide diversity of minerals with specific organic classes not specific to particular microbial groups. For instance, while here we see a primarily (lipo)polysaccharide signature associated with the fungal biooxides, proteins or proteinaceous material have also been documented as templates in fungal Mn oxide formation (Emerson et al., 1989). Conversely, the carbon associated with the bacterial Mn oxides here is dominated by proteins, but polysaccharides template Fe oxides associated with the sheath forming iron oxidizer *M. ferroxidans* (Chan, Fakra, Edwards, Emerson, & Banfield, 2009). Similarly, Mn oxide precipitates formed within biofilms of the bacterium *Psuedomonas putida* strain MnB1 were completely enveloped by the same polysaccharide material that comprised its biofilms, where this association was likely a combination of templated and adsorbed organic carbon (Toner, Fakra, Villalobos, Warwick, & Sposito, 2005). Clearly, this association of organic carbon and minerals does not appear to be unique to particular microbial groups and rather comprises a number of factors that may vary with lifestyle (e.g., surface associated vs. planktonic) and Mn oxidation pathway.

For the Mn(II)-oxidizing bacteria utilized in this study, the proteins involved in Mn(II) oxidation are sequestered and potentially preserved within the ensuing Mn oxide precipitates. Heme peroxidases and homologs, in particular, are among the most abundant mineral-hosted proteins within the *Roseobacter* and *Erythrobacter* Mn oxides and have been linked to both the direct and indirect (superoxide mediated) oxidation of Mn(II) by these organisms (Andeer et al., 2015; Anderson et al., 2009). Their presence in the mineral may be attributed to their additional function as a template (either passively or actively) or in inducing particle aggregation (Moreau et al., 2007). Alternatively, these proteins may play no role in particle formation or growth and instead may simply be adsorbed between particles and/or onto the Mn oxide surfaces. In fact, these heme peroxidases are the most abundant protein in both cell-free filtrate and the outer membrane fraction in *Roseobacter* AzwK-3b (Andeer et al., 2015; Learman &Hansel, 2014) and, thus, their prevalent association with the Mn oxides may simply be a function of their high abundance. Yet, minerals produced in both bacterial cultures harbor proteins specifically related to ion binding and transport of metals. Their metal-binding capability may lead to their preferential association with Mn(II) or Mn oxide particles. If so, carbon ultimately sequestered within biogenic Mn oxides may, in fact, provide some indication of the mechanism of Mn(II) oxidation and Mn oxide formation in some cases.

Similar to the bacterial cultures, Mn oxides formed in brackish Oyster Pond waters form in a C-rich environment and incorporate substantial quantities of OC into the mineral (Fig. 1). The OC associated with Mn oxides formed in incubation samples is dominated by aromatic, aliphatic, amide/carboxyl, and O-alkyl-C functional groups (Figs 5 and 6). Further, proteins are specifically observed associated with the Mn oxides formed in the water incubations (Fig. 1). As these Mn oxides were formed during active Mn(II) oxidation and oxide mineralization within the Oyster Pond water, we anticipate that, similar to the marine bacterial cultures, at least a proportion of this carbon is associated with the Mn(II)-oxidizing organisms responsible for Mn oxide formation within these waters. We further hypothesize that associated OC has additional sources not associated with the Mn(II) oxidation process, including biomass, POC, and DOC. Indeed, synthetic Mn oxides (as δ-MnO$_2$) directly incubated within Oyster Pond water contained substantial levels of OC, indicating that Mn oxides also passively adsorb or aggregate OC in these waters (Figs 2 and S2). By comparing the carbon associated with Mn oxides formed during active mineralization in the Oyster Pond water versus synthetic Mn oxides of similar structure added to the same water, ~44% of the OC associated with the biomineralized Mn oxides can be attributed to a solely passive adsorption reaction (see Fig. 2). Further, synthetic Mn oxides incubated in 0.2 μm filtered Oyster Pond water also accumulated OC, about ~50% as much as the OC in the unfiltered water, indicating that a substantial proportion of this mineral-associated OC derived from the dissolved pool (see Fig. 2). Given the initial DOC concentration of 0.74 ± 0.02 mmol DOC L^{-1} and an added concentration of 100 μM synthetic Mn oxide, we calculate that the Mn oxide-associated OC in that synthetic oxide + filtered water treatment represents ~4% of the initial DOC. This minor fraction of carbon removed within these carbon-rich coastal waters precludes robust quantification of Mn

oxide-induced compositional changes to the DOC pool or evidence for selective partitioning to the Mn oxides.

Thus, OC associated with the Mn oxides formed via biomineralization in Oyster Pond water likely reflects adsorption or incorporation of biomass and/or metabolites generated by Mn(II)-oxidizing microorganisms during Mn oxide formation as well as OC not associated with active Mn mineralization. Chen, Dynes, Wang, and Sparks (2014) observed an enrichment of aromatic C at low solid-phase OC:Fe ratios, similar to those OC:Mn ratios found in samples here. Eusterhues et al. (2011) examined fractionation of both polysaccharide-rich DOM and lignin material by ferrihydrite, observing that coprecipitation resulted in greater fractionation than adsorption only and that mineral-associated lignin material was enriched in aromatics relative to the original composition. Yet, aromatic C is not enriched in the Mn oxides formed during biomineralization in the Oyster Pond water; in fact, aromatic C comprises a significantly smaller percentage of the total fit area for biomineralized incubations than incubations of synthetic Mn oxides (Figs S4 and S5; Table S2), inverting what would be expected if these experiments truly represented 'adsorption-only' or 'coprecipitation-only' scenarios. This observation instead emphasizes that the chemical composition of OC associated with Mn oxides in incubation samples derives from a combination of source (microbial material, POC, DOC) and mineral-induced fractionation and that OC interacts with the mineral via several mechanisms.

In contrast to the low complexity and homogeneous nature of organic molecules associating with Mn oxides precipitated in cell-free filtrate of the bacterial and fungal cultures, Mn oxides formed in brackish Oyster Pond water and particularly in terrestrial caves bear OC that is more complex and spatially heterogeneous in chemical composition. Compared to culture-derived Mn oxides, C NEXAFS spectra extracted from regions within incubation and cave samples do not clearly match singular biomolecule standards, but contain instead a diversity of organic carbon functional groups. Although the proportions of the different functional groups vary both within regions of the same sample and between samples, all contain predominantly aromatic, aliphatic, amide/carboxyl, and O-alkyl C groups. The distribution of functional groups does not, in general, vary significantly between Mn oxides formed in cultures, brackish water, and terrestrial caves when peak fitting results from spectra are averaged by sample type (Fig. 4). Other studies of marine particles (Brandes et al., 2004) and soil aggregates (Lehmann et al., 2008) have found similar results, where different samples nonetheless contain the same classes of compounds.

One notable exception to the similarity in functional group distributions is an observed higher proportion of aliphatic C within the terrestrial cave samples (Fig. 9). Previous work has interpreted enrichment of aliphatic and amide C as evidence of microbial lipids and proteins that selectively partition onto mineral surfaces. Like this work, Keiluweit et al. (2012) found lipids and proteins intermixed within iron oxide-rich soils, while Liu et al. (2013) found lipids and proteins in separate 100–200 nm^2 domains after adsorption of extracellular polymeric substances to goethite. Mineral-associated OC in soil samples studied by Heckman et al. (2013) was dominated by polysaccharides, but also enriched in lipids and proteins which were

interpreted as microbial residues. The cave ferromanganese coatings, however, lack the O-alkyl-C enrichment that would be more indicative of polysaccharide material (as with the mycogenic oxides) and have a variable amide/carboxyl C content comparable to incubation and culture samples, suggesting a relatively higher lipid:protein content than that found in those previous studies on soil. The C-rich/no Mn regions (Fig. 7, BC regions 6 and 7, CL regions 8 and 9) are significantly enriched in aromatic and phenolic/ketonic groups (p = .01, two-tailed t test). These regions could represent the fraction of non-microbially processed, more terrestrial (lignin or otherwise plant derived) OC in the sample (Heckman et al., 2013) or intact fungal hyphae-like material (Keiluweit et al., 2012). Conversely, more Mn-rich regions could be interpreted as depleted in aromatics due to oxidative degradation by Mn oxides, as observed in Johnson et al. (2015) who documented preferential breaking of aromatic C–C bonds and conversion to low molecular weight compounds. However, as Mn-containing regions do not otherwise significantly differ from C-rich regions, we cannot conclusively attribute slight compositional differences to mineral-driven fractionation of microbial OC. Ultimately, the high aliphatic C content of cave Mn oxides may reflect differing C sources, differences in lifestyle (i.e. more lipid-rich biofilm formation for rock-associated microbes in cave systems), or a greater extent of microbial processing of OC. Given the oligotrophic cave environment and low measured carbon concentrations, this last option seems most feasible.

5 | CONCLUSIONS

Here, we show that manganese oxides harbor substantial concentrations of organic carbon that remain stable despite mineral ripening and particle aggregation (Figs S2 and S3). Biomolecules hosted within Mn oxides formed by bacteria and fungi are distinctly different, which could point to the potential for Mn oxide-hosted carbon as a biosignature. However, the concentration of OC associating with Mn oxides under different incubation conditions, in addition to the complex spectroscopic signature of OC within natural Mn oxides from the caves and brackish water incubations, suggests that environmental Mn oxides accumulate organic carbon from a range of sources through a range of mechanisms, which will overwrite any clear biomolecular signature.

Regardless of the OC source, Mn oxides sequester OC at substantial levels, as long appreciated for clay minerals and more recently Fe oxides. This association is established rapidly within cultures and brackish water incubations (Figs S2 and S3). Thus, Mn oxides may be an additional and important source and/or sink of OC within terrestrial and marine systems, including the subsurface or otherwise carbon-limited environments. In marine sediments or cave environments, Mn oxides may shuttle OC to depths where it is subsequently released and made bioavailable either by reductive dissolution of Mn oxide minerals, other diagenetic reactions, or an increased prevalence of exoenzymes that target the types of OC present at Mn oxide surfaces. Of particular interest is the attenuation and possible preservation of proteinaceous carbon within/on Mn oxide minerals (Figs 1 and 4, S2

and S3). If this preservation endures on time scales sufficiently greater than sedimentation and burial, then this mineral-hosted protein has the potential to fuel heterotrophic life in the deep subsurface. This brings up the intriguing possibility that mineral-derived proteins could explain the abundance of protein-degrading peptidases and protein-based metabolisms within some subsurface sediments (Lloyd et al., 2013). Conversely, if associated OC remains inaccessible to microbes and is stabilized over much longer time scales, Mn oxides may provide a mechanism for transferring organic carbon from the surface carbon cycle to the geological carbon cycle, facilitating burial and inhibiting remineralization. Moving forward, correlative approaches and microscale techniques will be invaluable for elucidating microzones representing different types of mineral–organic interactions within sediments and how the composition of Mn oxide-associated OC changes over time and throughout diagenesis.

REFERENCES

Andeer, P. F., Learman, D. R., McIlvin, M., Dunn, J. A., & Hansel, C. M. (2015). Extracellular haem peroxidases mediate Mn(II) oxidation in a marine Roseobacter bacterium via superoxide production. *Environmental Microbiology*, *17*, 3925–3936.

Anderson, C. R., Johnson, H. A., Caputo, N., Davis, R. E., Torpey, J. W., & Tebo, B. M. (2009). Mn(II) oxidation is catalyzed by heme peroxidases in "Aurantimonas manganoxydans" strain SI85-9A1 and Erythrobacter sp. strain SD-21. *Applied and Environmental Microbiology*, *75*, 4130–4138.

Arnarson, T. S., & Keil, R. G. (2001). Organic–mineral interactions in marine sediments studied using density fractionation and X-ray photoelectron spectroscopy. *Organic Geochemistry*, *32*, 1401–1415.

Bargar, J. R., Fuller, C. C., Marcus, M. A., Brearley, A. J., Perez De la Rosa, M., Webb, S. M., & Caldwell, W. A. (2009). Structural characterization of terrestrial microbial Mn oxides from Pinal Creek, AZ. *Geochimica et Cosmochimica Acta*, *73*, 889–910.

Bargar, J. R., Tebo, B. M., Bergmann, U., Webb, S. M., Glatzel, P., Chiu, V. Q., & Villalobos, M. (2005). Biotic and abiotic products of Mn(II) oxidation by spores of the marine Bacillus sp. strain SG-1. *American Mineralogist*, *90*, 143–154.

Berg, B., Davey, M. P., De Marco, A., Emmett, B., Faituri, M., Hobbie, S. E., … Virzo De Santo, A. (2010). Factors influencing limit values for pine needle litter decomposition: A synthesis for boreal and temperate pine forest systems. *Biogeochemistry*, *100*, 57–73.

Bock, M. J., & Mayer, L. M. (2000). Mesodensity organo – clay associations in a near-shore sediment. *Marine Geology*, *163*, 65–75.

Brandes, J. A., Lee, C., Wakeham, S., Peterson, M., Jacobsen, C., Wirick, S., & Cody, G. (2004). Examining marine particulate organic matter at sub-micron scales using scanning transmission X-ray microscopy and carbon X-ray absorption near edge structure spectroscopy. *Marine Chemistry*, *92*, 107–121.

Canfield, D. E., Thamdrup, B., & Hansen, J. W. (1993). The anaerobic degradation of organic matter in Danish coastal sediments: Iron reduction, manganese reduction, and sulfate reduction. *Geochimica et Cosmochimica Acta*, *57*, 3867–3883. Retrieved from http://www.ncbi.nlm.nih.gov/pubmed/11537734.

Carlson, C. A., Giovannoni, S. J., Hansell, D. A., Goldberg, S. J., Parsons, R., & Vergin, K. (2004). Interactions among dissolved organic carbon, microbial processes, and community structure in the mesopelagic zone of the northwestern Sargasso Sea. *Limnology and Oceanography*, *49*, 1073–1083.

Carmichael, M. J., Carmichael, S. K., Santelli, C. M., Strom, A., & Bräuer, S. L. (2013). Mn(II)-oxidizing bacteria are abundant and environmentally relevant members of ferromanganese deposits in caves of the Upper Tennessee River Basin. *Geomicrobiology Journal*, *30*, 779–800.

Carmichael, S., Carmichael, M. J., Strom, A., Johnson, K., Roble, L., Gao, Y., & Brauer, S. (2013). Sustained anthropogenic impact in Carter Saltpeter Cave, Carter County, Tennessee and the potential effects on manganese cycling. *Journal of Cave and Karst Studies*, *75*, 189–204.

Chan, C. S., Fakra, S. C., Edwards, D. C., Emerson, D., & Banfield, J. F. (2009). Iron oxyhydroxide mineralization on microbial extracellular polysaccharides. *Geochimica et Cosmochimica Acta*, *73*, 3807–3818.

Chan, C. S., Fakra, S. C., Emerson, D., Fleming, E. J., & Edwards, K. J. (2011). Lithotrophic iron-oxidizing bacteria produce organic stalks to control mineral growth: Implications for biosignature formation. *The ISME Journal*, *5*, 717–727.

Chen, C., Dynes, J. J., Wang, J., & Sparks, D. L. (2014). Properties of Fe-organic matter associations via coprecipitation versus adsorption. *Environmental Science & Technology*, *48*, 13751–13759.

Christie-Oleza, J. A., Piña-Villalonga, J. M., Bosch, R., Nogales, B., & Armengaud, J. (2012). Comparative proteogenomics of twelve Roseobacter exoproteomes reveals different adaptive strategies among these marine bacteria. *Molecular & Cellular Proteomics*, *11*, M111.013110. doi:10.1074/mcp.M111.013110

Claverys, J. P. (2001). A new family of high-affinity ABC manganese and zinc permeases. *Research in Microbiology*, *152*, 231–243.

Cowie, G. L., Hedges, J. I., Prahl, F. G., & de Lange, G. J. (1995). Elemental and major biochemical changes across an oxidation front in a relict turbidite: An oxygen effect. *Geochimica et Cosmochimica Acta*, *59*, 33–46.

Dick, G. J., Podell, S., Johnson, H. A., Rivera-Espinoza, Y., Bernier-Latmani, R., McCarthy, J. K., … Tebo, B. M. (2008). Genomic insights into Mn(II) oxidation by the marine alphaproteobacterium Aurantimonas sp. strain SI85-9A1. *Applied and Environmental Microbiology*, *74*, 2646–58.

Dickens, A. F., Baldock, J. A., Smernik, R. J., Wakeham, S. G., Arnarson, T. S., Gélinas, Y., & Hedges, J. I. (2006). Solid-state 13C NMR analysis of size and density fractions of marine sediments: Insight into organic carbon sources and preservation mechanisms. *Geochimica et Cosmochimica Acta*, *70*, 666–686.

Doetterl, S., Stevens, A., Six, J., Merckx, R., Van Oost, K., Pinto, M. C., … Boeckx, P. (2015). Soil carbon storage controlled by interactions between geochemistry and climate. *Nature Geoscience*, *8*, 780–783.

Dümig, A., Häusler, W., Steffens, M., & Kögel-Knabner, I. (2012). Clay fractions from a soil chronosequence after glacier retreat reveal the initial evolution of organo–mineral associations. *Geochimica et Cosmochimica Acta*, *85*, 1–18.

Ehrenreich, A., & Widdel, F. (1994). Anaerobic oxidation of ferrous iron by purple bacteria, a new-type of phototrophic metabolism. *Applied and Environmental Microbiology*, *60*, 4517–4526. Retrieved from <Go to ISI>://A1994PU39900042

Emerson, D., Garen, R. E., & Ghiorse, W. C. (1989). Formation of Metallogenium-like structures by a manganese-oxidizing fungus. *Archives of Microbiology*, *151*, 223–231.

Eusterhues, K., Rennert, T., Knicker, H., Kögel-Knabner, I., Totsche, K. U., & Schwertmann, U. (2011). Fractionation of organic matter due to reaction with ferrihydrite: Coprecipitation versus adsorption. *Environmental Science and Technology*, *45*, 527–533.

Flerus, R., Lechtenfeld, O. J., Koch, B. P., McCallister, S. L., Schmitt-Kopplin, P., Benner, R., … Kattner, G. (2012). A molecular perspective on the ageing of marine dissolved organic matter. *Biogeosciences*, *9*, 1935–1955.

Francis, C. A., Co, E., & Tebo, B. M. (2001). Enzymatic manganese (II) oxidation by a marine α-proteobacterium. *Applied and Environmental Microbiology*, *67*, 4024–4029.

Graham, S. C., Bond, C. S., Freeman, H. C., & Guss, J. M. (2005). Structural and functional implications of metal ion selection in aminopeptidase P, a metalloprotease with a dinuclear metal center. *Biochemistry*, *44*, 13820–13836.

Hansel, C. M., & Francis, C. A. (2006). Coupled photochemical and enzymatic Mn (II) oxidation pathways of a planktonic Roseobacter-Like bacterium. *Applied and Environmental Microbiology*, *72*, 3543–3549.

Heckman, K., Grandy, A. S., Gao, X., Keiluweit, M., Wickings, K., Carpenter, K., … Rasmussen, C. (2013). Sorptive fractionation of organic matter and formation of organo-hydroxy-aluminum complexes during litter biodegradation in the presence of gibbsite. *Geochimica et Cosmochimica Acta*, *121*, 667–683.

Heckman, K., Vazquez-Ortega, A., Gao, X., Chorover, J., & Rasmussen, C. (2011). Changes in water extractable organic matter during incubation of forest floor material in the presence of quartz, goethite and gibbsite surfaces. *Geochimica et Cosmochimica Acta*, *75*, 4295–4309.

Hedges, J. I., Baldock, J. A., Gélinas, Y., Lee, C., Peterson, M., & Wakeham, S. G. (2001). Evidence for non-selective preservation of organic matter in sinking marine particles. *Nature*, *409*, 801–804.

Henneberry, Y. K., Kraus, T. E. C., Nico, P. S., & Horwath, W. R. (2012). Structural stability of coprecipitated natural organic matter and ferric iron under reducing conditions. *Organic Geochemistry*, *48*, 81–89.

Hertkorn, N., Benner, R., Frommberger, M., Schmitt-Kopplin, P., Witt, M., Kaiser, K., … Hedges, J. I. (2006). Characterization of a major refractory component of marine dissolved organic matter. *Geochimica et Cosmochimica Acta*, *70*, 2990–3010.

Jiao, N., Herndl, G. J., Hansell, D. A., Benner, R., Kattner, G., Wilhelm, S. W., … Azam, F. (2010). Microbial production of recalcitrant dissolved organic matter: Long-term carbon storage in the global ocean. *Nature Reviews Microbiology*, *8*, 593–599.

Johnson, K., Purvis, G., Lopez-Capel, E., Peacock, C., Gray, N., Wagner, T., … Greenwell, C. (2015). Towards a mechanistic understanding of carbon stabilization in manganese oxides. *Nature Communications*, *6*, 7628.

Johnson, W. M., Soule, M. C. K., & Kujawinski, E. B. (2016). Evidence for quorum sensing and differential metabolite production by the marine heterotroph, Ruegeria pomeroyi, in response to DMSP. *The ISME Journal*, Advance online publication, 1–13. doi:10.1038/ismej.2016.6

Kaiser, K., & Guggenberger, G. (2000). The role of DOM sorption to mineral surfaces in the preservation of organic matter in soils. *Organic Geochemistry*, *31*, 711–725.

Keil, R. G., Montluçon, D. B., Prahl, F. G., & Hedges, J. I. (1994). Sorptive preservation of labile organic matter in marine sediments. *Nature*, *370*, 549–552.

Keiluweit, M., Bougoure, J. J., Nico, P. S., Pett-Ridge, J., Weber, P. K., & Kleber, M. (2015). Mineral protection of soil carbon counteracted by root exudates. *Nature Climate Change*, 5, 588–595.

Keiluweit, M., Bougoure, J. J., Zeglin, L. H., Myrold, D. D., Weber, P. K., Pett-Ridge, J., ... Nico, P. S. (2012). Nano-scale investigation of the association of microbial nitrogen residues with iron (hydr)oxides in a forest soil O-horizon. *Geochimica et Cosmochimica Acta*, 95, 213–226.

Keiluweit, M., Nico, P., Harmon, M. E., Mao, J., Pett-Ridge, J., & Kleber, M. (2015). Long-term litter decomposition controlled by manganese redox cycling. *Proceedings of the National Academy of Sciences*, 112, E5253–E5260.

Kleber, M., Eusterhues, K., Keiluweit, M., Mikutta, C., Mikutta, R., & Nico, P. S. (2015). Mineral-organic associations: Formation, properties, and relevance in soil environments. *Advances in Agronomy*, 130, 1–140.

Kleber, M., Nico, P. S., Plante, A., Filley, T., Kramer, M., Swanston, C., & Sollins, P. (2011). Old and stable soil organic matter is not necessarily chemically recalcitrant: Implications for modeling concepts and temperature sensitivity. *Global Change Biology*, 17, 1097–1107.

Koebnik, R., Locher, K. P., & Van Gelder, P. (2000). Structure and function of bacterial outer membrane proteins: Barrels in a nutshell. *Molecular Microbiology*, 37, 239–253.

Krumbein, W. E., & Altmann, H. J. (1973). A new method for the detection and enumeration of manganese oxidizing and reducing microorganisms. *Helgoländer Wissenschaftliche Meeresuntersuchungen*, 25, 347–356.

Kuddus, M., & Ramteke, P. W. (2008). A cold-active extracellular metalloprotease from Curtobacterium luteum (MTCC 7529): Enzyme production and characterization. *The Journal of General and Applied Microbiology*, 54, 385–392.

Lalonde, K., Mucci, A., Ouellet, A., & Gélinas, Y. (2012). Preservation of organic matter in sediments promoted by iron. *Nature*, 483, 198–200.

Learman, D. R., & Hansel, C. M. (2014). Comparative proteomics of Mn(II)-oxidizing and non-oxidizing Roseobacter clade bacteria reveal an operative manganese transport system but minimal Mn(II)-induced expression of manganese oxidation and antioxidant enzymes. *Environmental Microbiology Reports*, 6, 501–509.

Learman, D. R., Wankel, S. D., Webb, S. M., Martinez, N., Madden, A. S., & Hansel, C. M. (2011). Coupled biotic–abiotic Mn(II) oxidation pathway mediates the formation and structural evolution of biogenic Mn oxides. *Geochimica et Cosmochimica Acta*, 75, 6048–6063.

Lechtenfeld, O. J., Kattner, G., Flerus, R., McCallister, S. L., Schmitt-Kopplin, P., & Koch, B. P. (2014). Molecular transformation and degradation of refractory dissolved organic matter in the Atlantic and Southern Ocean. *Geochimica et Cosmochimica Acta*, 126, 321–337.

Lehmann, J., Solomon, D., Kinyangi, J., Dathe, L., Wirick, S., & Jacobsen, C. (2008). Spatial complexity of soil organic matter forms at nanometre scales. *Nature Geoscience*, 1, 238–242.

Liu, X., Eusterhues, K., Thieme, J., Ciobota, V., Höschen, C., Mueller, C. W., ... Totsche, K. U. (2013). STXM and NanoSIMS investigations on EPS fractions before and after adsorption to goethite. *Environmental Science & Technology*, 47, 3158–3166.

Lloyd, K. G., Schreiber, L., Petersen, D. G., Kjeldsen, K. U., Lever, M. A., Steen, A. D., ... Jørgensen, B. B. (2013). Predominant archaea in marine sediments degrade detrital proteins. *Nature*, 496, 215–218.

Lu, X., & Zhu, H. (2005). Tube-gel digestion: A novel proteomic approach for high throughput analysis of membrane proteins. *Molecular & Cellular Proteomics*, 4, 1948–1958.

Mann, S., Archibald, D. D., Didymus, J. M., Douglas, T., Heywood, B. R., Meldrum, F. C., & Reeves, N. J. (1993). Crystallization at inorganic-organic interfaces: Biominerals and biomimetic synthesis. *Science*, 261, 1286–1292.

Moreau, J. W., Weber, P. K., Martin, M. C., Gilbert, B., Hutcheon, I. D., & Banfield, J. F. (2007). Extracellular proteins limit the dispersal of biogenic nanoparticles. *Science*, 316, 1600–1603.

Ostolaza, H., Soloaga, A., & Goni, F. M. (1995). The binding of divalent cations to *Escherichia coli* alpha-haemolysin. *European Journal of Biochemistry*, 228, 39–44.

Picard, A., Kappler, A., Schmid, G., Quaroni, L., & Obst, M. (2015). Experimental diagenesis of organo-mineral structures formed by microaerophilic Fe(II)-oxidizing bacteria. *Nature Communications*, 6, 6277.

Poulton, S. W., & Raiswell, R. (2005). Chemical and physical characteristics of iron oxides in riverine and glacial meltwater sediments. *Chemical Geology*, 218, 203–221.

Ransom, B., Kim, D., Kastner, M., & Wainwright, S. (1998). Organic matter preservation on continental slopes: Importance of mineralogy and surface area. *Geochimica et Cosmochimica Acta*, 62, 1329–1345.

Roy, M., McManus, J., Goñi, M. A., Chase, Z., Borgeld, J. C., Wheatcroft, R. A., ... Mix, A. (2013). Reactive iron and manganese distributions in seabed sediments near small mountainous rivers off Oregon and California (USA). *Continental Shelf Research*, 54, 67–79.

Santelli, C. M., Pfister, D. H., Lazarus, D., Sun, L., Burgos, W. D., & Hansel, C. M. (2010). Promotion of Mn(II) oxidation and remediation of coal mine drainage in passive treatment systems by diverse fungal and bacterial communities. *Applied and Environmental Microbiology*, 76, 4871–4875.

Santelli, C. M., Webb, S. M., Dohnalkova, A. C., & Hansel, C. M. (2011). Diversity of Mn oxides produced by Mn(II)-oxidizing fungi. *Geochimica et Cosmochimica Acta*, 75, 2762–2776.

Schumacher, M., Christl, I., Scheinost, A. C., Jacobsen, C., & Kretzschmar, R. (2005). Chemical heterogeneity of organic soil colloids investigated by scanning transmission X-ray microscopy and C-1s NEXAFS microspectroscopy. *Environmental Science & Technology*, 39, 9094–100. Retrieved from http://www.ncbi.nlm.nih.gov/pubmed/16382929.

Solomon, D., Lehmann, J., Kinyangi, J., Liang, B., & Schafer, T. (2005). Carbon K-Edge NEXAFS and FTIR-ATR Spectroscopic Investigation of organic carbon speciation in soils. *Soil Science Society of America Journal*, 69, 107–119. Retrieved from https://dl.sciencesocieties.org/publications/sssaj/abstracts/69/1/0107

Solomon, D., Lehmann, J., Kinyangi, J., Liang, B., Heymann, K., Dathe, L., ... Jacobsen, C. (2009). Carbon (1s) NEXAFS spectroscopy of biogeochemically relevant reference organic compounds. *Soil Science Society of America Journal*, 73, 1817.

Stone, A., & Morgan, J. (1984). Reduction and dissolution of manganese(III) and manganese(IV) oxides by organics: 2. Survey of the reactivity of organics. *Environmental Science & Technology*, 18, 617–624. Retrieved from http://pubs.acs.org/doi/pdf/10.1021/es00126a010.

Sunda, W., & Kieber, D. (1994). Oxidation of humic substances by manganese oxides yields low-molecular-weight organic substrates. *Nature*, 367, 62–64. Retrieved from http://www.nature.com/nature/journal/v367/n6458/abs/367062a0.html.

Tebo, B. M., Bargar, J. R., Clement, B. G., Dick, G. J., Murray, K. J., Parker, D., ... Webb, S. M. (2004). Biogenic manganese oxides: Properties and mechanisms of formation. *Annual Review of Earth and Planetary Sciences*, 32, 287–328.

Toner, B. M. B., Fakra, S. S. C., Manganini, S. S. J., Santelli, C. M., Marcus, M. A., Moffett, J. W., ... Edwards, K. J. (2009). Preservation of iron(II) by carbon-rich matrices in a hydrothermal plume. *Nature Geoscience*, 2, 197–201.

Toner, B., Fakra, S., Villalobos, M., Warwick, T., & Sposito, G. (2005). Spatially resolved characterization of biogenic manganese oxide production within a bacterial biofilm. *Applied and Environmental Microbiology*, 71, 1300–1310.

Van Waasbergen, L. G., Hoch, J. A., & Tebo, B. M. (1993). Genetic analysis of the marine manganese-oxidizing Bacillus sp. strain SG- 1: Protoplast transformation, Tn917 mutagenesis, and identification of chromosomal loci involved in manganese oxidation. *Journal of Bacteriology*, 175,

7594–7603. Retrieved from: http://jb.asm.org/content/175/23/7594. short.

Villalobos, M., Toner, B., Bargar, J., & Sposito, G. (2003). Characterization of the manganese oxide produced by pseudomonas putida strain MnB1. *Geochimica et Cosmochimica Acta*, *67*, 2649–2662.

Webb, S. M. (2005a). SIXpack: A graphical user interface for XAS analysis using IFEFFIT. *Physica Scripta*, *T115*, 1011–1014.

Webb, S. M. (2005b). Structural characterization of biogenic Mn oxides produced in seawater by the marine bacillus sp. strain SG-1. *American Mineralogist*, *90*, 1342b–1357.

Zeiner, C. A. (2015). Role of the secretome in manganese and carbon oxidation by filamentous ascomycete fungi. *Doctoral thesis* Harvard University, Cambridge, MA, USA.

SUPPORTING INFORMATION

Additional Supporting Information may be found online in the supporting information tab for this article.